# Electronic structure characterization and bandgap engineering of solar hydrogen materials

Jinghua Guo

Advanced Light Source, Lawrence Berkeley National Laboratory, Berkeley, CA 94720

## ABSTRACT

Bandgap, band edge positions as well as the overall band structure of semiconductors are of crucial importance in photoelectrochemical and photocatalytic applications. The energy position of the band edge level can be controlled by the electronegativity of the dopants, the pH of the solution (flatband potential variation of 60 mV per pH unit), as well as by quantum confinement effects. Accordingly, band edges and bandgap can be tailored to achieve specific electronic, optical or photocatalytic properties. Synchrotron radiation with photon energy at or below 1 keV is giving new insight into such areas as condensed matter physics and extreme ultraviolet optics technology. In the soft x-ray region, the question tends to be, what are the electrons doing as they migrated between the atoms. In this paper, I will present a number of soft x-ray spectroscopic study of nanostructured *3d* metal compounds $Fe_2O_3$ and ZnO.

**Key words:** synchrotron radiation, electronic structure, photon-in/photon-out in-situ study, X-ray absorption,

## 1. INTRODUCTION

Solar energy can be converted to heat for warming space and water, to electricity and chemical fuels for energy use and storage [1-4]. However, the cost and conversion efficiency have hampered the potential use of solar energy. There are the emerging technologies of using semiconductors for light harvesting assemblies; and charge transfer processes to solar cells. Sunlight in the near infrared, visible, and near ultraviolet regions has considerable energy (about 0.9 to 3.2 electron volts per photon) and intensity. It could provide a significant contribution to our electrical and chemical resources if efficient and inexpensive systems utilizing readily available materials could be devised for the conversion process.

The electron-hole pair formation that occurs at the interface between a semiconductor and a solution upon absorption of light leads to oxidation or reduction of solution species. The fabrication of artificial photosynthetic systems for the conversion of $H_2O$ and $CO_2$ to fuels (for examples, $H_2$ and $CH_3OH$) has become a field of much current research interest and has encouraged new fundamental investigations of the interactions of light, electron flow, and chemical reactions.

Bandgap, band edge positions as well as the overall band structure of semiconductors are of crucial importance in photoelectrochemical and photocatalytic applications. The energy position of the band edge level can be controlled by the electronegativity of the dopants, solution pH (for example, flatband potential variation of 60 mV per pH unit), as well as by quantum confinement effects. Accordingly, the band edges and bandgap can be tailored to achieve specific electronic, optical or photocatalytic properties in nanostructure semiconductors.

Synchrotron radiation based soft-x-ray spectroscopy has recently become a useful tool to determine the bandgap properties of semiconductors [5,6]. X-ray originates from an electronic transition between a localized core state and a valence state. Soft-x-ray absorption probes the local *unoccupied* electronic structure (conduction band); soft-x-ray emission probes the *occupied* electronic structure (valence band); and the addition of resonant inelastic soft-x-ray scattering (Raman spectroscopy with soft x-rays) can tell the energy levels that reflect the chemical and physical properties of semiconductors. Recently, quantum size effects on the exciton and band-gap energies were observed in semiconductor nanocrystals [7-9]. If the observed valence band (VB) or conduction band (CB) shifts are due to quantum confinement, one would expect the size of the band shifts to increase as the particle size of the nanocrystals is decreased.

A very important application was found in the generation of $H_2$ from direct photo-oxidation of water without external bias

[10-12]. Indeed, to succeed in splitting water via solar irradiation only, the valence band of the semiconductor has to be located at a lower energy level than the chemical potential of oxygen evolution ($H_2O/O_2$), and the conduction band has to be located at a higher energy level than the chemical potential of hydrogen evolution ($H_2/H^+$). If the position of the energy levels of the valence and conduction band is not fulfilled, an external bias has to be applied to induce the photocatalytic process, which in turn substantially reduces the overall efficiency.

It has been reported that the minimum bandgap of 2.46 eV is required for water photo-oxidation without an external bias [13]. Although the bandgap of hematite, reported to be around 1.9 to 2.2 eV (depending on its crystalline status and methods of preparation), and its valence band edge are suitable for oxygen evolution, the conduction band edge of hematite is too low to generate hydrogen. Therefore, a blue shift of the bandgap of hematite of about 0.3 to 0.6 eV and the concomitant upward shift of the conduction band edge would make hematite an ideal anode material for photocatalytic devices for the photo-oxidation of water in terms of the cost, abundance, non-toxicity, as well as thermal and structural stability and photo-corrosion resistance.

## 2. PHOTON-IN/PHOTON-OUT SOFT-X-RAY SPECTROSCOPY

Soft-x-ray absorption probes the local unoccupied electronic structure, soft-x-ray emission probes the occupied electronic structure, and the introduction of resonant inelastic soft-x-ray scattering opens a new field of study by disclosing many new possibilities of photon-in/photon-out soft-x-ray spectroscopy.

Photon-in/photon-out soft-x-ray spectroscopy offers a number of unique features, which we will utilize in the proposed research. Element and chemical site specific probing based on the tunability of synchrotron radiation. This is a valuable general asset in study of complex hydrides, and often important for the study of nano-structured materials. Photons are insensitive to external fields and partially also insensitive to a gaseous environment. This allows for the investigation of real materials in the photoelectrochemical reactions or under a controlled hydrogen atmosphere and selected temperature. Resonant inelastic scattering implies independence of the core hole lifetime broadening, and thus offers a unique opportunity to utilize very high resolution in the study of the changes in the electronic structure, for example the opening of a gap, associated with phase transitions, doping or nano fabrications. In short, soft-x-ray spectroscopy offers a high degree of information selectivity on electronic properties with respect to atomic species, chemical site, symmetry, and local order.

## 3. EXPERIMENTAL SETUP

Beamline 7.0 is equipped with a SGM monochromator providing resolving power of 4000 in energy range of 80-1000 eV available for studying the fundamental electronic properties. Figure 1 shows the Soft-X-Ray Fluorescence (SXF) endstation and samples in different phases can be handled. The beamline and endstation are capable for performing XAS measurement, and a high resolution grating spectrometer is used for XES and RIXS studies.

Fundamental understanding of hydrogen storage processes calls for the in-situ study capability of soft-x-ray spectroscopy. To exploit the possibility of in-situ characterization, we built the liquid cell and hydrogen reaction cell that will allow the demonstration of the hydrogen reaction under a range of temperature and pressure. In soft-x-ray regime, the attenuation length of photons is typically hundreds of nanometers in solid matter. The penetration depth offers the experimental opportunities not present in electron based spectroscopy. We have demonstrated the soft-x-ray spectroscopic studies of liquids, gases, and solid samples in a gaseous environment, for example to examine the influence of the intermolecular interaction on the local electronic structure of liquid water and methanol [14,15].

A sample hydrogen cell is provided with an entrance window and an exit window for incident photons and emitted photons, respectively. The cell is connected to a hydrogen manifold outside the vacuum system by means of flexible meal hoses. The entrance window is about 0.2 mm in diameter and typically made of 100-nm silicon nitride or carbon, and the exit window is typically polyimide of same thickness. The hydrogen cell is capable of holding atmospheric pressure.

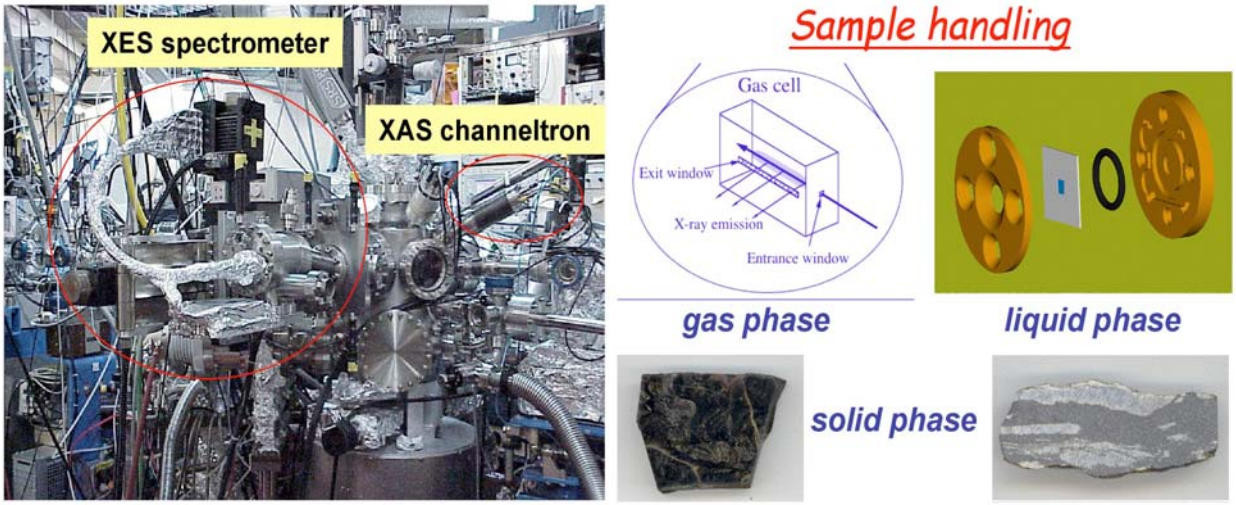


Figure 1. The SXF endstation and sample handling at BL7.0.

## 4. CHEMICAL SENSITIVITY OF SOFT-X-RAY SPECTROSCOPY

Chemical sensitivity is obtained when the resolution of the detected emission lines is high enough to resolve fine structure. The line shapes are determined by the valence electron distribution and the transitions are governed by dipole selection rules. For solids, essentially a partial density of state (DOS) mapping is obtained. This is exemplified by the carbon K-edge absorption and emission spectra of the carbon solids.

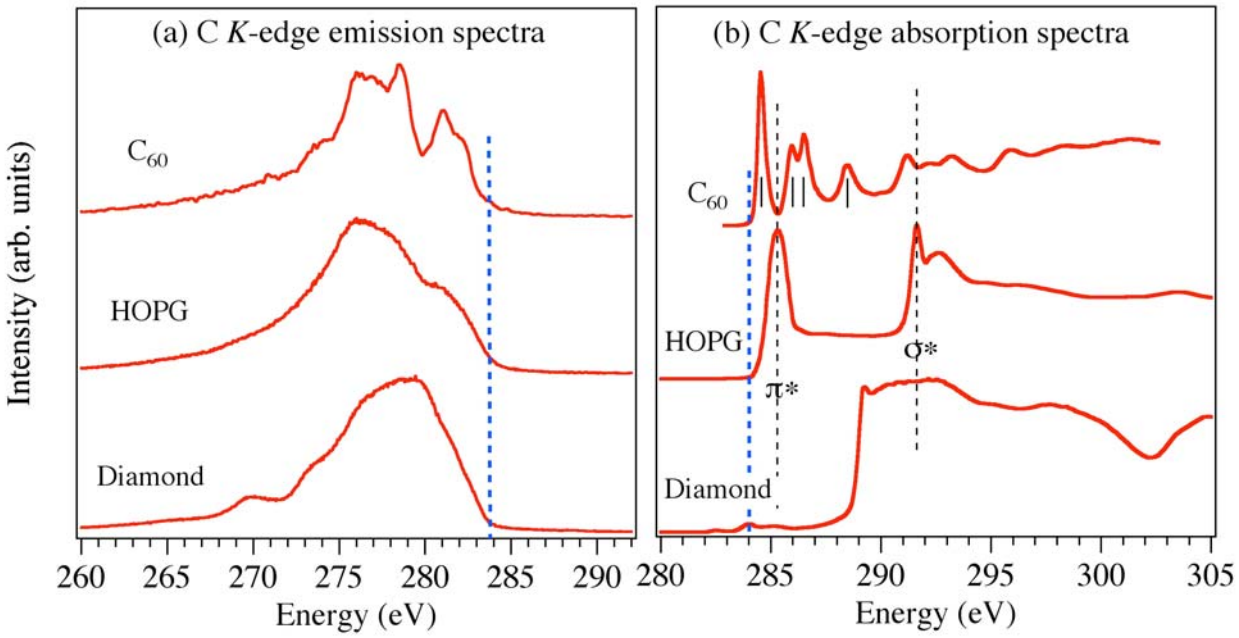


Figure 2. Non-resonant carbon K-edge emission spectra of $C_{60}$, amorphous carbon (graphitic), and diamond (a); X-ray absorption spectra of $C_{60}$, HOPG, and diamond (b).

The difference in structural arrangement of these carbon forms gives rise to the wide differences in their physical properties. Carbon has an atomic number of 6 and has the $1s^2 2s^2 2p^2$ configuration in its electronic ground states. The sp-orbital, and the $sp^3$-hybrid orbital indicate rotational symmetry. Bonds of this kind are call π-bonds. The electrons involved in such bonds are called π-electrons. With double bonds, so-called σ-orbitals occur with corresponding σ -electrons. Such orbitals are not symmetrical with regard to their bonding orientation.

The normal carbon K-edge x-ray and absorption and emission spectra of $C_{60}$, HOPG, and diamond presented in Figure 2, where large differences in spectral profile are observed. The spectra of diamond and graphitic carbon show a wide band with some shoulder structures, where the energy positions of the peak maximum and band shapes are largely different. In some studies related to vapor deposition the X-ray emission spectral profile has been used as a means to identify certain chemical states [16]. The X-ray absorption spectrum of diamond shows no π* contribution, and the absorption feature at 288.9 eV is the diamond exciton. In contrast, the spectra of $C_{60}$ exhibit clearly resolved emission peaks, indicating strong molecular character in their solid phase. The marked band edges show the large bandgap in diamond in contrast to metallic behavior of graphite.

## 5. BANDGAP AND DOPING

The electronic structure of insulator $YBa_2Cu_3O_{6.02}$ and superconductors $YBa_2Cu_3O_{6.94}$ was studied with a combination of XAS and XES [17]. The O 1*s* absorption spectra of $YBa_2Cu_3O_{6.02}$ and $YBa_2Cu_3O_{6.94}$, which reflect the unoccupied O 2*p* states, are shown in Figure 3. The absorption prepeak in $YBa_2Cu_3O_{6.02}$ starting from 530 eV is attributed to the covalent mixing states of O 2*p*–Cu 3*d*. The XAS spectrum of $YBa_2Cu_3O_{6.94}$ shows a strong increase of the intensity at the lower binding energy region. This behavior is similar to that in the O 1*s* absorption edges of other cuprates [18,19], which is due to the doping-induced shift of the Fermi level into the valence band, the creation of the holes in the valence band, and a transfer of spectral weight from states in the upper Hubbard band to the upper edge of the valence band.

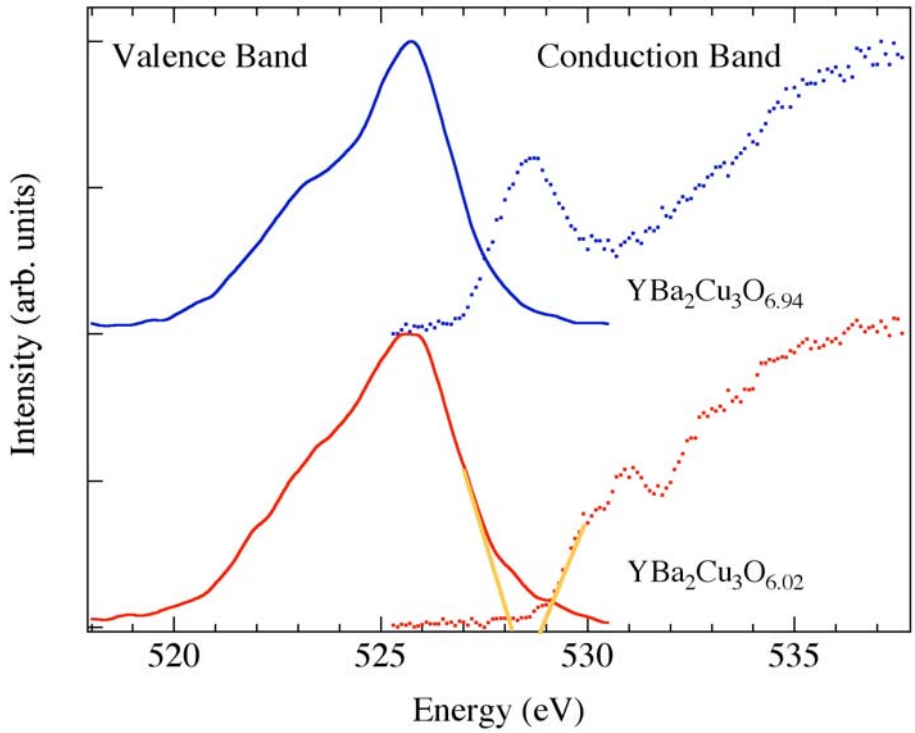


Figure 3. Resonantly (534.7 eV) and normal (545.5 eV) excited XES spectra of liquid water in comparison with calculations for SYM, A-ASYM and D-ASYM species. Excitation energies are marked in the XAS spectrum.

The valence-core XES spectra of the two samples are aligned together with the corresponding XAS spectra. The XES spectra are similar to those obtained with conventional x-ray emission spectroscopy in prior studies. An absorption prepeak appearing at 528.5 eV in the O 1*s* absorption spectrum of $YBa_2Cu_3O_{6.94}$ indicates the transferring of spectral weight from states in the upper Hubbard band to the upper edge of the valence band, and the *absorption-emission* spectrum shows the continuing density of states crossing the Fermi level, reflecting the metallic character of $YBa_2Cu_3O_{6.94}$. In contrast, a band gap is observed in $YBa_2Cu_3O_{6.02}$. The top of the valence band locates about the same position for both cuprates, so the closing down of the band gap in $YBa_2Cu_3O_{6.02}$ is seen as the moving down of the bottom of the conduction band.

The O *K*-edge absorption and emission spectra of $FePO_4$ and $LiFePO_4$ are plotted on a common energy scale in Figure 4. Both XES spectra of $FePO_4$ and $LiFePO_4$ show four resolved emission bands with some differences in the intensity distribution and central weight for bands $E_1$ and $E_3$. An increase in intensity of $E_2$ is observed in $LiFePO_4$, while the deeper emission band $E_4$ is less affected by Li intercalation. A small weight of enhancement is also found at the top of the valence band starting from 528 eV of $LiFePO_4$. X-ray-absorption spectra show a main threshold starting from absorption feature $A_4$ for both $FePO_4$ and $LiFePO_4$. The pre-edge absorption features are indicated as $A_1$ and $A_2$, which are clearly resolved in $FePO_4$ in contrast to a broadband in $LiFePO_4$. The nature of the absorption features of $A_1$ and $A_2$ will be interpreted in the later paragraph. A notable intensity increase in the region of $A_3$ is also observed in $LiFePO_4$, which is probably related to the Li intercalation,

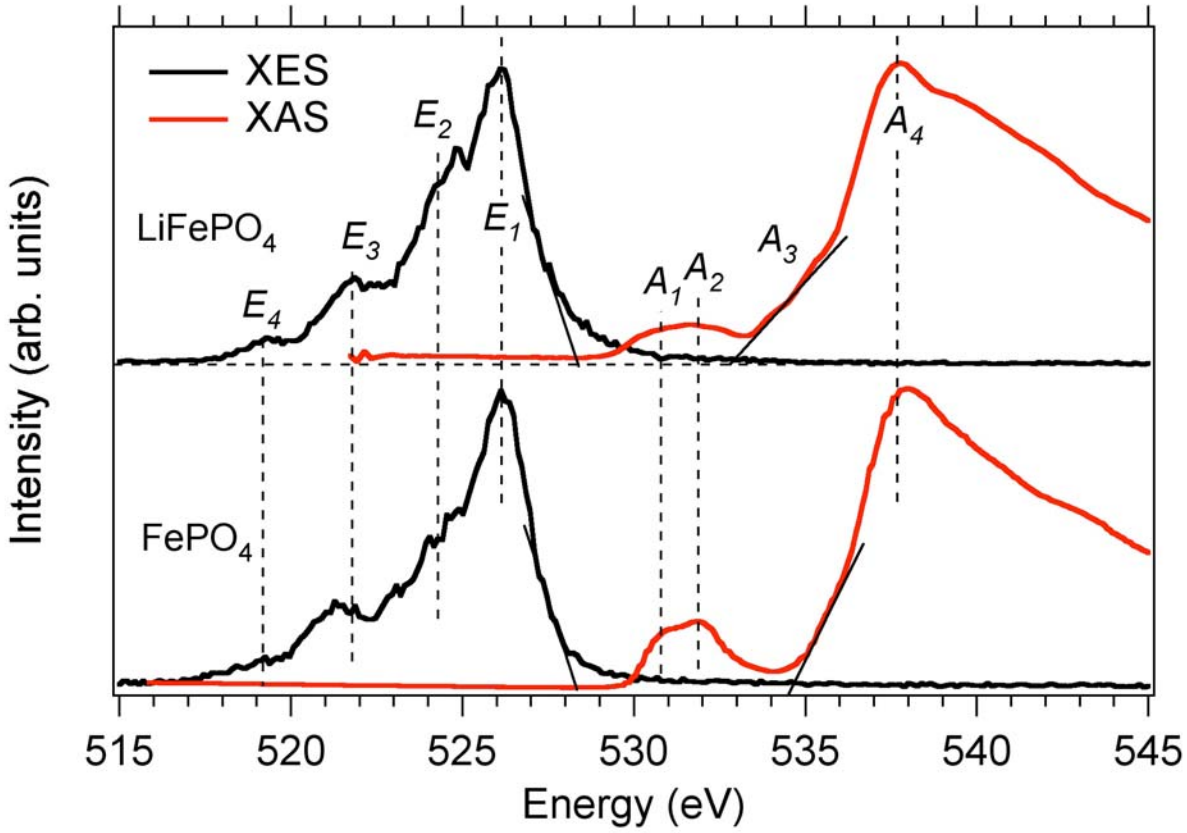


Figure 4. X-ray absorption-emission spectra of $FePO_4$ and $LiFePO_4$.

The last example shows that a combined x-ray absorption-emission spectrum offers an alternative method for measuring the band gaps of insulators and semiconductors. However, it is difficult to determine the band gap in $FePO_4$ and $LiFePO_4$ from current XAS and XES study. The determination of the top of the valence band is clear as indicated in Figure 4. If one assigns the Fe-3*d*–O-2*p* hybridized states to be the bottom of the conduction band, the band gap obtained would be 1.7 and 0.5 eV for $FePO_4$ and $LiFePO_4$, respectively. But if one assigns the Li-derived state in O *K*-edge absorption spectrum of $LiFePO_4$ to be the bottom of the conduction band, a band gap of 4.0 eV is obtained for $LiFePO_4$, which

agrees well with the theoretical value. Thus, the states in the band gap of $LiFePO_4$ indicated as $A_1$ and $A_2$ in x-ray-absorption spectrum would be excitonic in nature.

Characteristic changes in the valence and conduction bands are observed upon delithation of $LiFePO_4$ into $FePO_4$. In $LiFePO_4$, the Fe-3*d* states are localized with little overlap with the O-2*p* states. Delithiation of $LiFePO_4$ gives stronger hybridization between Fe-3*d* states and O-2*p* states leading to delocalization of the O-2*p* states.

## 6. BANDGAP AND NANOSTRUCTURE MATERIALS

Soft x-ray spectroscopy has found its usefulness in probing the electronic structure of nanostructured solids [5]. The development of the electronic band structure of solids from discrete localized atomic state is one of the key points of interest. As the size of nanocrystal extended into a truly molecular regime, the optical bandgap for the semiconducting nanocrystal increases.

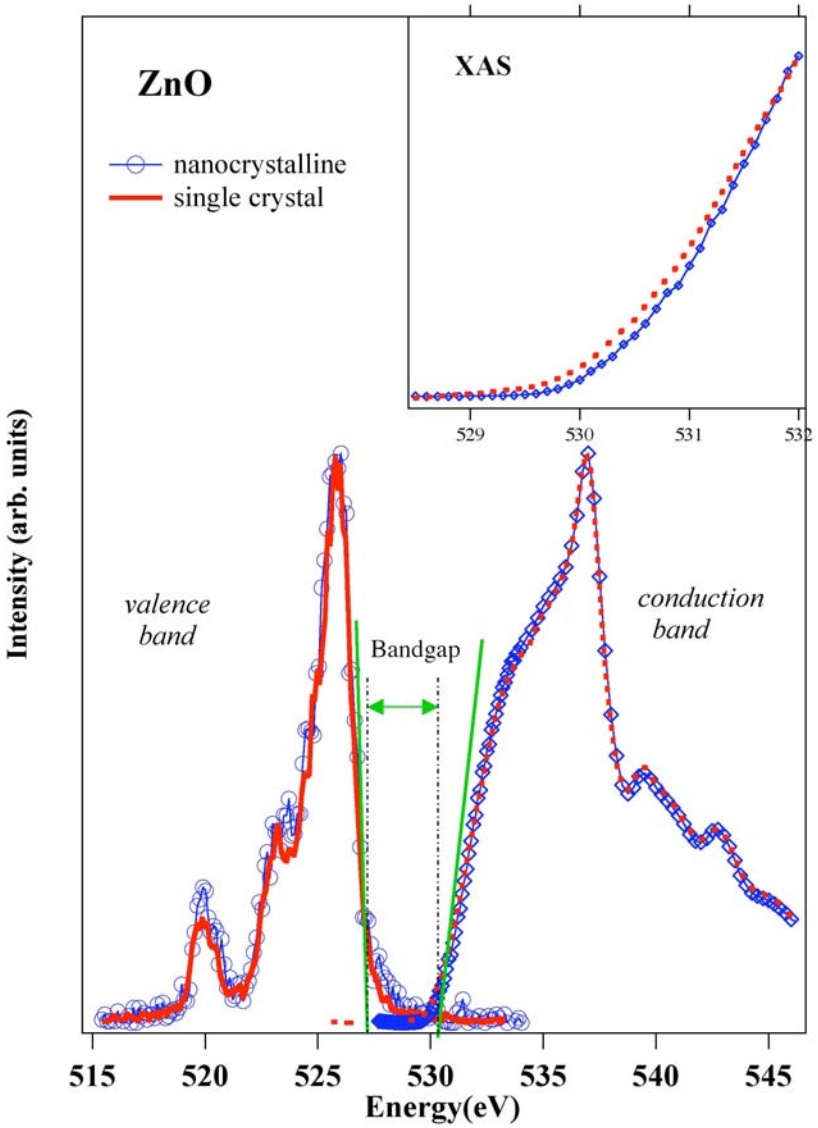


Figure 5. XAS and XES spectra of bulk and nanocrystalline ZnO.

ZnO, a wide band-gap semiconductor, has attracted a considerable attention during the last years due to its potential technological applications. The XES spectra of bulk and nanotructured ZnO are displayed together with the corresponding XAS spectrum in Figure 5 [20]. The O K-edge emission spectrum reflects the O 2p occupied states (valence band), and the O K-edge absorption spectrum reflects the O 2p unoccupied states (conduction band). In the photon energy region of 530-539 eV, the X-ray absorption can be mainly assigned to the O 2p hybridized with Zn 4s states. In the region of 539-550 eV the spectrum is mainly attributed to O 2p hybridized with Zn 4p states. Above 550 eV, the contribution is mainly coming from O 2p - Zn 4d mixed states [21]. Stronger hybridization was revealed in nanostructured ZnO since the contributions of features at 520 eV and 523 eV are enhanced. The O *K*-emission of the valence band shows that the Zn 3*d*–O 2*p* mixed states lie about 7 eV below the valence-band maximum.

A well-defined band-gap can be observed between the valence-band maximum and conduction-band minimum. Our absorption-emission spectrum yields the fundamental band-gap energy of 3.3 eV. The inset show nanocrystalline (100 nm) ZnO gives a little larger bandgap due to the surface structure.

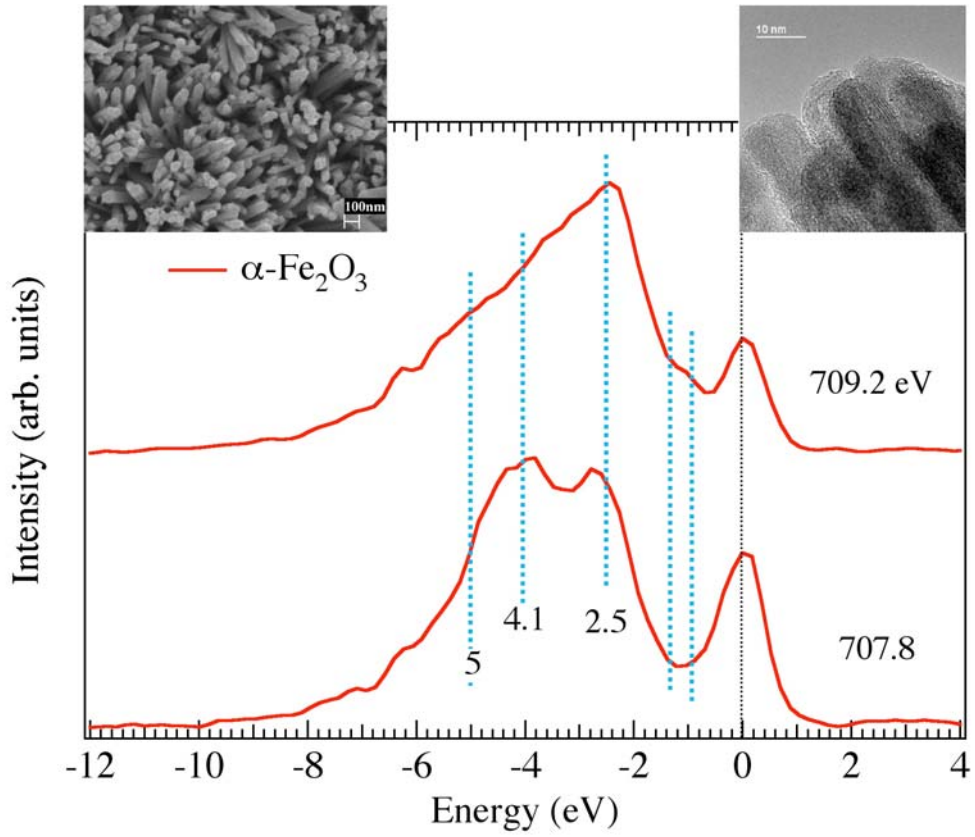


Figure 6. Energy dependent resonant inelastic soft-x-ray scattering spectra of α-$Fe_2O_3$ nanorod-arrays. Upper two insets are the electron microscopy images of α-$Fe_2O_3$ arrays consisting of oriented and bundled ultrafine nanorods.

Figure 6 shows the investigation of quantum confinement effects on bandgap profiling in similar arrays by resonant inelastic soft-x-ray scattering of synchrotron radiation for potential application of such nanomaterials in direct photo-oxidation of water by solar irradiation. The 2.5-eV excitation [22], which corresponds to the bandgap transition of hematite, appears significantly blue shifted compared to the reported 1.9~2.2 eV bandgap of single-crystal and polycrystalline samples. Such finding strongly suggests that such designed nanomaterials would meet the bandgap requirement for the photocatalytic oxidation of water without an applied bias.

## ACKNOWLEDGEMENTS

I would like to acknowledge the contributions from my collaborators: J.-W. Chiou, C. L. Dong, L. Vayssieres, etc. The Advanced Light Source is supported by the Director, Office of Science, Office of Basic Energy Sciences, of the U.S. Department of Energy under Contract No. DE-AC02-05CH11231.

## REFERENCES

1. George W. Crabtree and Nathan S. Lewis, "Solar Energy Conversion", Physics Today, March 2007. doi:10.1063/1.2718755
2. James R. Bolton, Stewart J. Strickler, and John S. Connolly, "Limiting and realizable efficiencies of solar photolysis of water", Nature **316**, 495 (1985). doi:10.1038/316495a0
3. Allen J. Bard, "Photoelectrochemistry", Science **207**, 139 (1980). doi: 10.1126/science.207.4427.139
4. James R. Bolton, Solar Fuels, Science **202**, 705 (1978). doi: 10.1126/science.202.4369.705
5. Jinghua Guo, "Synchrotron radiation, soft-X-ray spectroscopy and nanomaterials", Int. J. Nanotechnology **1-2**, 193-225 (2004). Doi: 10.1504/IJNT.2004.003729
6. Jinghua Guo, "X-ray Absorption and Emission Spectroscopy in Nanoscience and Lifesciences", pp. 259-291, in *Nanosystem characterization Tools in the Life Sciences*, edited by Challa Kumar, Wiley-VCH Verlag GmbH & Co. KgaA, Weinheim (March 2006).
7. T. van Buuren, L. N. Dinh, L. L. Chase, W. J. Siekhaus, and L. J. Terminello, "Changes in the Electronic Properties of Si Nanocrystals as a Function of Particle Size", Phys. Rev. Lett. **80**, 3803 (1998). doi: 10.1103/PhysRevLett.80.3803
8. K. S. Hamad, R. Roth, J. Rockenberger, T. van Buuren, and A. P. Alivisatos, "Structural Disorder in Colloidal InAs and CdSe Nanocrystals Observed by X-Ray Absorption Near-Edge Spectroscopy", Phys. Rev. Lett. **83**, 3474 (1999). doi: 10.1103/PhysRevLett.83.3474
9. Jean-Yves Raty, Giulia Galli, C. Bostedt, Tony van Buuren, and Louis J. Terminello, "Quantum Confinement and Fullerenelike Surface Reconstructions in Nanodiamonds", Phys. Rev. Lett. **90**, 37401 (2003). doi: 10.1103/PhysRevLett.90.037401
10. Akira Fujishima and Kenichi Honda, "Electrochemical Photolysis of Water at a Semiconductor Electrode", Nature **238**, 37 (1972). doi:10.1038/238037a0
11. Tooru Inoue, Akira Fujishima, Satoshi Konishi, Kenichi Honda, "Photoelectrocatalytic reduction of carbon dioxide in aqueous suspensions of semiconductor powders", Nature **277**, 637 (1979). doi:10.1038/277637a0
12. Z. Zhou, J. Ye, K. Sayama, and H. Arakawa, "Direct splitting of water under visible light irradiation with an oxide semiconductor photocatalyst", *Nature* **414**, 625 (2001). doi:10.1038/414625a
13. Y. Matsumoto, "Energy Positions of Oxide Semiconductors and Photocatalysis with Iron Complex Oxides", *J. Solid-State Chem.* **126**, 227 (1996). doi:10.1006/jssc.1996.0333
14. J.-H. Guo, Y. Luo, A. Augustsson, J.-E. Rubensson, C. Såthe, H. Ågren, H. Siegbahn, and J. Nordgren, "X-ray Emission Spectroscopy of Hydrogen Bonding and Electronic Structure of Liquid Water", Phys. Rev. Lett. **89**, 137402 (2002)
15. J.-H. Guo, Y. Luo, A. Augustsson, S. Kashtanov, J.-E. Rubensson, D. K. Shuh, H. Agren, and J. Nordgren, "The molecular structure of alcohol-water mixtures", Phys. Rev. Lett. **91**, 157401 (2003)
16. J.-H. Guo and J. Nordgren, "Resonant C *Ka* X-ray emission of some carbon allotropes and organic compounds", J. Electron Spectrosc. Relat. Phenom. 110-111, 105-134 (2000)
17. J.-H. Guo, S.M. Butorin, N. Wassdahl, P. Skytt, J. Nordgren, Y. Ma, P. Berastegut, and L.-G. Johansson, "The Character of Unoccupied States in $YBa_2Cu_3O_x$ Studied by Soft X-ray Fluorescence Spectroscopy with Tunable Excitation", Phys. Rev. B **61**, 9140 (2000).
18. J.-H Guo, S. M. Butorin, N. Wassdahl, P. Skytt, J. Nordgren, and Y. Ma, "Electronic Structure of $La_{2-x}Sr_xCuO_4$ Studied by Soft X-ray Fluorescence Spectroscopy with Tunable Excitation", Phys. Rev. B 49, 1376 (1994).
19. S. M. Butorin, J.-H. Guo, N. Wassdahl, P. Skytt, J. Nordgren, Y. Ma, C. Ström, G. Johansson, and M. Qvarford, "On the Electronic Structure of $Bi_2Sr_2CaCu_2O_{8+d}$ and $Tl_2Ba_2CaCu_2O_8$", Phys. Rev. B 51, 11915 (1995).
20. C. L. Dong, C. Persson, L. Vayssieres, A. Augustsson, T. Schmitt, M. Mattesini, R. Ahuja, C. L. Chang, and J.-H. Guo, "Electronic structure of nanostructued ZnO from x-ray absorption and emission spectroscopy and local density approximation", Phys. Rev. B **70**, 195325 (2004).

21. J.-H. Guo, L. Vayssieres, C. Persson, R. Ahuja, B. Johansson, and J. Nordgren, “Polarization-dependent soft-x-ray absorption of highly oriented ZnO microrod arrays”, J. Phys.: Condens. Matter 14, 6969-6974 (22 July 2002).
22. L. Vayssieres, C. Såthe, S. M. Butorin, D. K. Shuh, J. Nordgren, and J.-H. Guo, “One-Dimensional Quantum-Confinement Effect in a-$Fe_2O_3$ Ultrafine Nanorod Arrays”, Adv. Mater. **17**, 2320 (2005). doi: 10.1002/adma.200500992

*jguo@lbl.gov; phone 1 510 495-2230; fax 1 510 495-2067